

Phase diagram and effective shape of semi-flexible colloidal rods and biopolymers

M. Dennison,¹ M. Dijkstra,¹ and R. van Roij²

¹*Soft Condensed Matter, Debye Institute for Nanomaterials Science, Utrecht University, Princetonplein 5, 3584 CC Utrecht, The Netherlands*

²*Institute for Theoretical Physics, Utrecht University, Leuvenlaan 4, 3584 CE Utrecht, The Netherlands*

(Dated: October 8, 2018)

We study suspensions of semi-flexible colloidal rods and biopolymers using an Onsager-type second-virial functional for a segmented-chain model. For suspensions of thin and thick fd virus particles we calculate phase diagrams in quantitative agreement with experimental observations, and we find their effective state-point dependent shape to be much shorter and thicker than the actual shape. We also calculate the stretching of worm-like micelles in a host fd virus solution, again finding agreement with experiments. For both systems, our results show that the fd virus stiffness can play a key role in system behavior.

Rod-like particles are capable of forming a great variety of liquid-crystalline phases [1], and have been widely explored experimentally and theoretically [2]. Recently a prominent role is being played by aqueous suspensions of fd virus particles, which are charged, semi-flexible, Brownian needles with a length-to-diameter ratio exceeding 100, exhibiting isotropic (I), cholesteric nematic (N), smectic, columnar, and crystalline phases upon increasing the concentration [3–5]. Moreover, wild-type fd virus particles have been bio-engineered to have, for instance, a polyethylene-glycol (PEG) coating, such that mixtures of thin and thick rods with diameter ratios d varying from 1.1 to 3.7 could be studied experimentally [6]. The resulting experimental phase diagrams are extremely rich, even in the regime where only I and N phases are relevant. For instance, the observations not only include I-N coexistence with strong fractionation effects, but also, for $d \gtrsim 3$, two-phase N-N and three-phase I-N-N coexistence with phase diagram topologies that strongly depend on d . Given the needle-like shape of the fd virus particles, and the relative structural simplicity of I and N phases, one would expect these phase diagrams to be well understood, e.g. resembling those of theoretical predictions based on Onsager’s second virial theory for thin-thick mixtures of rigid rods [7]. However, these systems turn out to be surprisingly poorly understood. For instance, the experiments show N-N demixing with a low-density (lower) critical point that shifts to lower densities with increasing d [6], while the theory predicts the exact opposite: a high-density (upper) N-N critical point and N-N demixing that extends to higher densities with increasing d [7]. Moreover, the experiments show N-N demixing at diameter ratios as low as $d \gtrsim 2 - 3$ while rigid-rod models predict $d \gtrsim 4 - 5$ [6, 7]. In this Letter we will show that the key to a real understanding of these systems is *flexibility*, which renders the needles effectively shorter and fatter depending on the state point [8, 9]. In addition, our model and theory can also quantify the observed *stretching* of guest biopolymers in host suspensions of fd virus particles [10].

One-component systems of semi-flexible rods have been studied using numerous methods, and it is known that only a slight flexibility is enough to shift the I-N transition to significantly higher concentrations [11–15]. We build on the segmented-chain model introduced by Wessels and Mulder [15], in which (i) flexibility is incorporated by introducing a bending potential between the chain segments, and (ii) excluded volume is taken into account at the segment level. This approach reproduces (in the appropriate limits) the results of Ref. [11], with the advantage of only having to deal with a discrete number of degrees of freedom, making explicit calculations of extensions to two-component systems feasible.

We consider a suspension of N_i semi-flexible rods of species $i = 1, 2$ with contour lengths L_i , in a volume V at temperature T . Following Ref. [15] we model a rod of species i as a chain of M_i rod-like segments of length $l_i = L_i/M_i$ and diameter $D_i \ll l_i$. Denoting the orientation of the m -th segment by a unit-vector ω_m (with $1 \leq m \leq M_i$), we write the bending energy of a chain of species i with orientation $\Omega = \{\omega_1, \dots, \omega_{M_i}\}$ as

$$U_i(\Omega) = \sum_{m=1}^{M_i-1} u_i(\omega_m, \omega_{m+1}) = -\frac{P_i}{l_i} \sum_{m=1}^{M_i-1} \omega_m \cdot \omega_{m+1}, \quad (1)$$

where the stiffness is described in terms of the persistence length P_i [15]. Here and below we use thermal energy units by setting $k_B T = 1$. The state of the suspension is characterized by the orientation distribution functions (ODFs) $f_i(\Omega)$, which satisfy the normalization condition $\int d\Omega f_i(\Omega) = 1$ where $d\Omega = \prod_{m=1}^{M_i} d\omega_m$. Denoting the total number of rods by $N = N_1 + N_2$, the density by $\rho = N/V$, and the mole fraction of species i by $x_i = N_i/N$, we can write the variational free-energy functional $F[f_1, f_2]$ within an Onsager-like second virial approximation as

$$\frac{F}{N} = \ln(B\rho) - 1 + x_1 \ln x_1 + x_2 \ln x_2 \quad (2)$$

$$\begin{aligned}
& + \sum_{i=1}^2 x_i \int f_i(\boldsymbol{\Omega}) \left(\ln(4\pi f_i(\boldsymbol{\Omega})) + U_i(\boldsymbol{\Omega}) \right) d\boldsymbol{\Omega} \\
& + \frac{\rho}{2} \sum_{i,j=1}^2 x_i x_j \int f_i(\boldsymbol{\Omega}) f_j(\boldsymbol{\Omega}') K_{ij}(\boldsymbol{\Omega}, \boldsymbol{\Omega}') d\boldsymbol{\Omega} d\boldsymbol{\Omega}'.
\end{aligned}$$

The first line of Eq. (8) represents the translational and the mixing ideal-gas contributions (with $B = \frac{\pi}{4} D_1 L_1^2$, a constant), the second line, the orientation entropy and bending energy, and the third line the excluded volume interactions, which can be considered at the segment level with $K_{ij}(\boldsymbol{\Omega}, \boldsymbol{\Omega}') = \sum_{m=1}^{M_i} \sum_{m'=1}^{M_j} k_{ij}(\omega_m, \omega_{m'})$. The free-energy functional in Eq. (8) is a two-component generalization of the one-component segmented-chain functional of Ref. [15], and for $M_i = 1$ and $U_i \equiv 0$ it reduces to the Onsager functional for binary mixtures of rigid rods [7, 16]. From hereon, we simply summarize our method, and direct those interested in the complete outline to the appendix. At a given thermodynamic state point, the equilibrium ODFs minimize F and therefore satisfy

$$f_i(\boldsymbol{\Omega}) = \frac{\exp(-U_i(\boldsymbol{\Omega}) - V_i(\boldsymbol{\Omega}))}{Q_i}; \quad (3)$$

$$V_i(\boldsymbol{\Omega}) = \rho \sum_{j=1}^2 x_j \int K_{ij}(\boldsymbol{\Omega}, \boldsymbol{\Omega}') f_j(\boldsymbol{\Omega}') d\boldsymbol{\Omega}', \quad (4)$$

where $V_i(\boldsymbol{\Omega})$ can be seen as a self-consistent field acting on all segments of a chain, and Q_i is a partition function-like normalization factor [15]. Explicitly solving Eqs. (10) and (11) for state points of interest would be prohibitively expensive computationally because of the high-dimensional angular $\boldsymbol{\Omega}$ -grids that would be required in the case when $M_i \gg 1$. Instead, we formally evaluate the functional F of Eq. (8) in its minimum by inserting the solutions f_i of Eqs. (10) and (11) to find the equilibrium free energy

$$\begin{aligned}
\frac{F_{\text{Eq}}}{N} & = \ln(B\rho) - 1 + x_1 \ln \frac{x_1}{Q_1} + x_2 \ln \frac{x_2}{Q_2} - \frac{1}{2} \rho \sum_{i,j} x_i x_j \\
& \times \sum_{m=1}^{M_i} \sum_{m'=1}^{M_j} \int k_{ij}(\omega, \omega') f_{i,m}(\omega) f_{j,m'}(\omega') d\omega d\omega', \quad (5)
\end{aligned}$$

where $f_{i,m}(\omega)$ is the ODF of the m -th segment ($m = 1, \dots, M_i$) of a chain of species $i = 1, 2$ given by $f_{i,m}(\omega) = \int f_i(\boldsymbol{\Omega}) \delta(\omega - \omega_m) d\boldsymbol{\Omega}$. Eq. (12) implies that the thermodynamics does *not* require the full solutions $f_i(\boldsymbol{\Omega})$ but only the M_i single-segment distributions $f_{i,m}(\omega)$ and the normalization factors Q_i . The calculation of these is given in the appendix. With the ODFs, and hence F_{Eq} , known, all thermodynamic properties such as osmotic pressure Π and phase diagrams follow [7].

We have calculated the phase diagrams for mixtures of bare fd particles (species 1, thin) and PEG-coated ones (species 2, thick), with equal contour and persistence lengths, $L_1 = L_2 = 0.88 \mu\text{m}$ and $P_1 = P_2 = 2.2 \mu\text{m}$

[6]. The bare fd diameter is fixed to $D_1 = 6.6 \text{nm}$, and following the experiments of Ref. [6] we consider several diameter ratios $d = D_2/D_1$ to describe varying thicknesses of the PEG coating. Throughout, we use sufficient segments per virus particle such that we are in the continuum limit for all state points of interest (see the appendix). In Fig. 1 we show, for several d , the resulting phase diagrams in the (η_1, η_2) representation, where η_i denotes the packing fraction of species $i = 1, 2$. For all d we find isotropic-nematic (I-N) coexistence, with the tie-lines indicating, for increasing d , an increasing fractionation of the thinner and thicker rods preferentially into the I and N phase, respectively.

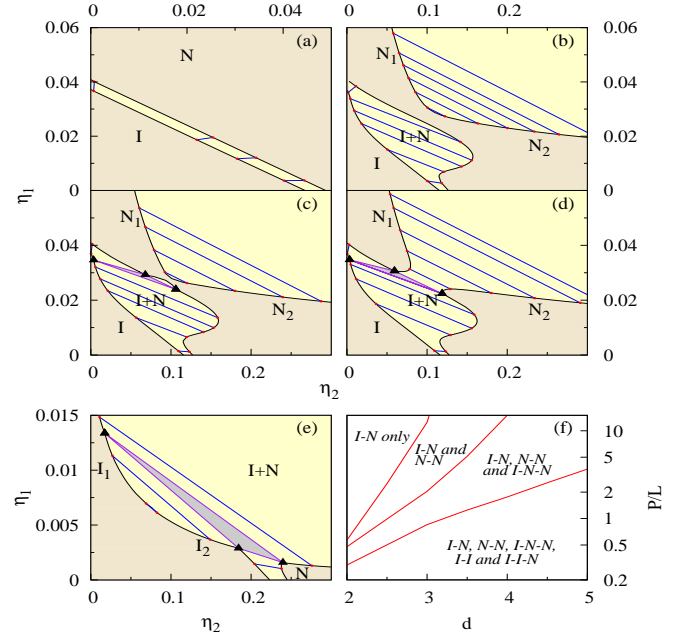


FIG. 1. Phase diagrams (see text) for mixtures of bare (thin) fd virus particles (species 1) and PEG-coated (thick) ones (species 2), with diameter ratios (a) $d = 1.2$, (b) 3.1, (c) 3.11, (d) 3.125, (e) 6. The lighter colored areas indicate the two-phase regions with tie-lines connecting coexisting state-points; triangles denote I-N-N and I-I-N triple points. (f) Topology of the phase diagram (two- and three phase coexistence) of binary mixtures of (modified) fd virus particles as a function of their diameter ratio d and persistence length P .

In agreement with the experiments of Ref. [6] we find *no* N-N coexistence in the density regime of interest for the smallest diameter ratio $d = 1.2$ (Fig. 1(a)). For increasing d an N-N demixing regime appears in the density regime of interest, with a *lower* critical point as shown for $d = 3.1$ in Fig. 1(b); in the experiments of Ref. [6] such a phase diagram was found for $d \simeq 2.9$. Slightly increasing the PEG layer thickness to $d = 3.11$ reveals an I-N-N triple point and an associated N-N demixing regime with an *upper* critical point emerging out of the I-N coexistence regime (Fig. 1(c)). This N-N upper critical point has not been reported experimentally, perhaps

because it only exists in a small regime of diameter ratios: for $d = 3.125$ (Fig. 1(d)) the upper and lower N-N points have merged to form a single neck-shaped N-N regime that is separated from the I-N coexistence regime by an I-N-N triple point, with the I and one N phase rich in bare fd-particles and the other N phase rich in PEG-coated fd-particles. Interestingly, such neck-shaped phase diagrams have *also* been reported in Ref. [6] for diameter ratios $d \simeq 3$. For $d = 6$, Fig. 1(e) shows an I-I-N triple point and I-I coexistence, as found also for thin-thick mixtures of rigid rods with diameter ratios exceeding $d \simeq 8$ [7]. We find that this behavior is present for $d \gtrsim 4.5$.

Motivated by recent progress in the bio-engineering of fd virus particles [17], which may allow for tuning their flexibility, we have also calculated binary-mixture phase diagrams for a large variety of diameter ratios and persistence lengths $P_1 = P_2 \equiv P$. Fig. 1(f) summarizes our findings by dividing the (d, P) plane into regimes with phase diagrams featuring only an I-N transition (for stiff rods and small d) all the way to complex phase diagrams with I-N, I-I, N-N phase coexistence and I-I-N and I-N-N triple points (for flexible rods and large d). Clearly, increasing d and decreasing P have similar effects on the phase diagram, and hence increasing the flexibility is expected to considerably enhance the complexity of the phase diagrams.

In order for a model system of rigid rods to fully capture the phase behavior of binary fd virus systems, one must use a system of much shorter, thicker rods, with $L/D \lesssim 7$ for the PEG-coated fd virus [6], much lower than the true values of 20 – 110. The inference is that long semi-flexible rods exhibit the same phase behavior as short rigid rods [8, 9]. Our model also enables us to study the effective shape exhibited by the flexible rods throughout the binary fd virus systems. We define the mean square effective length $L_{e,i}^2$ as

$$L_{e,i}^2 = l_i^2 \sum_{m=1}^{M_i} \sum_{m'=1}^{M_i} \int (\omega \cdot \omega') f_{i,m,m'}(\omega, \omega') d\omega d\omega', \quad (6)$$

where $f_{i,m,m'}(\omega, \omega')$ is the pair orientation distribution function (PDF), the calculation for which is given in the appendix. We use the PDFs to calculate $L_{e,i}$ and, from this, the effective diameter $D_{e,i}$ required for rigid rods of length $L_{e,i}$ to have the same excluded volume as flexible rods of length L_i .

Fig. 2(a) shows the effective shape of the rods $L_{e,i}/D_{e,i}$, for a mixture of thick-thin fd virus particles with $d = 3$, throughout the phase diagram (the route we follow is shown in Fig. 2(b), where we use the $x_2 - \Pi$ representation for clarity). What is immediately apparent is that throughout the phase diagram, while the rods always behave as shorter, thicker rods, the effective shape varies considerably. In the isotropic phase, we find $L_{e,i}/D_{e,i}$ to be about 20% of L_i/D_i (for both species).

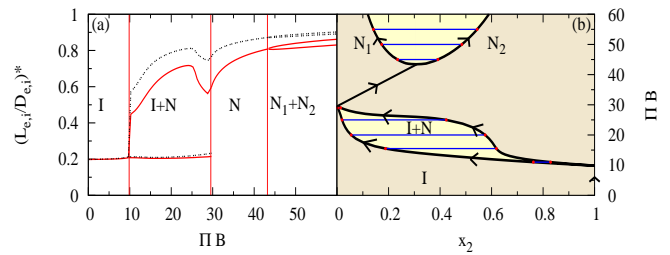


FIG. 2. (a) Relative effective shape $(L_{e,i}/D_{e,i})^* = (L_{e,i}/D_{e,i})/(L_i/D_i)$ of fd virus particles as a function of osmotic pressure (Π) (solid lines show bare fd, dashed lines show PEG-coated fd), and (b) the path we follow throughout the phase diagram in the $x_2 - \Pi$ representation, indicated by the arrows.

This corresponds to $L_e/D_e \approx 8.5$ for the thick rods, close to the $L/D \lesssim 7$ required for rigid rod systems to capture the phase behavior of these binary systems [6]. For the nematic phase, however, $L_{e,i}/D_{e,i}$ jumps to over 50% of L_i/D_i , and increases considerably as Π is increased. We conclude that a fixed effective shape does not capture the essential physics of these suspensions; the state-point dependent stretching of the flexible rods is a key feature.

Finally, we present results for the effective length of semi-flexible polymers dissolved in an fd virus suspension. A range of polymers which undergo a coil-rod transition, stretching out over the I-N transition of the host fd virus, has been studied experimentally [10]. Here, we examine worm-like micelles, which have constant $P = 0.5 \mu\text{m}$, $D = 14 \text{nm}$ and variable $L = 5 - 50 \mu\text{m}$. The concentration of the polymers is sufficiently low that they can be treated as a single particle in a bulk fd virus suspension, and we study the behavior of the polymer L_e over the I-N phase transition of the fd virus (which is at $\Pi B = 29.54$). The results are shown in Fig. 3(a). For the shortest polymers studied, we see a considerable jump in L_e , from $L_e \simeq 0.26L$ to $\simeq 0.61L$, corresponding to a coil-rod transition. For longer polymers, the jump in L_e becomes smaller, and the longest ones only become truly rod-like well into the nematic phase of the fd virus. It is interesting to note that in the isotropic phase, for all cases, L_e appears to remain essentially constant.

In the isotropic fd virus phase, the polymer may be considered along the lines of the Kratky-Porod worm-like chain model [18], generalized to account for excluded volume effects [19]. The average end-to-end length is defined as $L_{KP} = \sqrt{4P'P}(L/2P)^\nu$, where P' is an effective persistence length. For an ideal Kratky-Porod chain $P' = P$ and $\nu = 0.5$. We calculate L_e in the isotropic phase ($L_{e,I}$) for a large range of L values, and fit L_{KP} to our results for the range of worm-like micelle parameters. We find $P' = 0.573P$, and $\nu = 0.529$, shown in Fig. 3(b), where we also compare our results to the ideal Kratky-Porod worm-like chain, and to the rigid rod length L . Clearly, for shorter micelles, $L_{e,I}$ approaches L , whilst

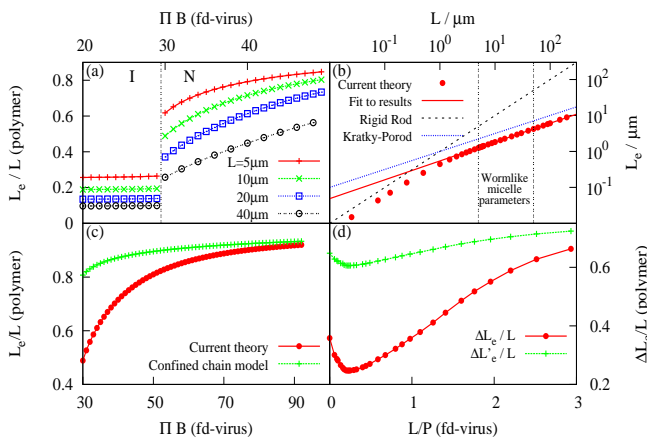


FIG. 3. (a) L_e of worm-like micelles of various L against host fd virus osmotic pressure Π . (b) $L_{e,I}$ against L , with fit to L_{KP} , compared to the ideal Kratky-Porod L_{KP} and rigid rod L . (c) $L_{e,N}$ of worm-like micelles with $L = 10\mu\text{m}$, and L_O of a confined semi-flexible polymer, against Π . (d) ΔL_e of worm-like micelles against L/P of host fd virus, compared to $\Delta L'_e$

for longer ones, $L_{e,I}$ approaches the ideal Kratky-Porod L_{KP} .

In the nematic fd virus phase, we can consider the polymer using the Odijk confined worm-like chain model [14], where the host nematic acts as a confining cylinder. The average end-to-end length is defined as $L_O = L\langle\omega \cdot \mathbf{n}\rangle$, proportional to the average $\omega \cdot \mathbf{n}$ along the chain, where \mathbf{n} is the nematic director. We find that our calculated effective length at the I-N phase transition $L_{e,N}$ is significantly below L_O (Fig. 3(c)), from which we infer that the host nematic is neither dense nor ordered enough to fully confine the polymer. By altering the stiffness of the host fd virus such that it is denser (flexible fd virus) or more ordered (rigid) at the transition (see the appendix), we may confine better the polymer causing it to stretch out more over the I-N transition. Fig. 3(d) shows $\Delta L_e = L_{e,N} - L_{e,I}$ for worm-like micelles of $L = 10\mu\text{m}$, using a range of P values for the fd virus. Here we see that ΔL_e is the largest when using the most flexible fd virus and it decreases as the fd virus becomes more rigid, until it reaches a minimum, before increasing again for the most rigid fd virus studied. This presents the opportunity to tune the stretching of the polymers by varying the stiffness of the host fd virus. We also compare ΔL_e to $\Delta L'_e = L_O - L_{KP}$ (Fig. 3(d)), finding that this overestimates ΔL_e , but does qualitatively match our non-monotonic results.

In conclusion, we have developed a model for binary mixtures of semi-flexible rods, and applied it to binary fd virus mixtures. We find I-N, N-N (with upper, lower and no critical points) and I-N-N coexistence regions present in such systems, consistent with experimental results [6]. Additionally, we have shown that the N-N upper critical

point only exists in a very small diameter ratio regime, which may explain why it has never been seen experimentally. For systems with diameter ratios larger than those studied experimentally so far, we also find I-I and I-I-N coexistence regions. We also see that altering the stiffness of the rods can have the same effect on phase behavior as altering the diameter ratio, giving an extra parameter to tuning the phase behavior of rod-like particles. The addition of flexibility in our model gives results that are quantitatively closer to experimental observations than those obtained using rigid rods [6]. The key reason appears to lie in the effective shape of the rods, which changes throughout the phase diagrams, indicating that any static-shaped rigid rod model will miss some of the essential physics. We have also studied the stretching of semi-flexible polymers in an fd virus solvent. We find that sufficiently short polymers stretch out considerably over the I-N transition of the host solvent, while for the longer ones, some stretching is observed, but the effect is much less pronounced. Changing the stiffness of the host fd virus, such that the density or nematic order at the I-N transition is increased, can greatly increase the stretching effect. We hope that our findings will stimulate further experimental explorations, and believe that extensions of the theory to e.g. inhomogeneous states and non-equilibrium phenomena are within reach of the present model.

Financial support of a FOM and a NWO-VICI grant is acknowledged.

-
- [1] S. Chandrasekhar, *Liquid Crystals 2nd edition* (Cambridge University Press, 1993).
 - [2] G. J. Vroege and H. N. W. Lekkerkerker, Rep. Prog. Phys. **55**, 1241 (1992).
 - [3] J. Tang and S. Fraden, Liq. Cryst. **19**, 459 (1995).
 - [4] Z. Dogic and S. Fraden, Philos. Trans. R. Soc. London Ser. A **359**, 997 (2001).
 - [5] E. Grelet, Phys. Rev. Lett. **100**, 168301 (2008).
 - [6] K. R. Purdy, S. Varga, A. Galindo, G. Jackson, and S. Fraden, Phys. Rev. Lett. **94**, 057801 (2005).
 - [7] R. van Roij, B. Mulder, and M. Dijkstra, Physica A **261**, 374 (1998).
 - [8] H. Fynewever and A. Yethiraj, J. Chem. Phys. **108**, 1636 (1998).
 - [9] A. N. Semenov and A. V. Subbotin, Polymer Science **31**, 2266 (1989).
 - [10] Z. Dogic *et al.*, Phys. Rev. Lett. **92**, 125503 (2004).
 - [11] A. R. Khokhlov and A. N. Semenov, Physica A **108**, 546 (1981); **112**, 605 (1982).
 - [12] Z. Y. Chen, Macromolecules **26**, 3419 (1993).
 - [13] M. Dijkstra and D. Frenkel, Phys. Rev. E **51**, 5891 (1995).
 - [14] T. Odijk, Macromolecules **19**, 2313 (1986).
 - [15] P. P. F. Wessels and B. M. Mulder, Soft Materials **1**, 313 (2003); J. Phys. Cond. Matt. **18**, 9335 (2006).
 - [16] G. J. Vroege and H. N. W. Lekkerkerker, J. Phys. Chem.

- 97**, 3601 (1993).
- [17] E. Barry, D. Beller, and Z. Dogic, *Soft Matter* **5**, 2563 (2009).
- [18] O. Kratky and G. Porod, *J. Colloid. Sci.* **4**, 35 (1949).
- [19] H.-P. Hsu, W. Paul, and K. Binder, *Macromolecules* **43**, 3094 (2010).
- [20] L. Onsager, *Ann. N.Y. Acad. Sci.* **51**, 627 (1949).
- [21] B. Tjpto-Margo and G. T. Evans, *J. Chem. Phys.* **93**, 4254 (1990).
- [22] R. F. Kayser and H. J. Raveché, *Phys. Rev. A* **17**, 2067 (1978).
- [23] R. van Roij, *Eur. J. Phys.* **26**, S57 (2005).

APPENDIX

Theory

Free-energy minimization and phase diagrams

In the Onsager theory [20], the isotropic-nematic phase transition of a one-component system of rigid-rods is driven by competition between two entropies. One is similar to entropy of mixing, arising from the mixing of particles of different orientations. The other arises from the excluded volume interactions of the particles. These are expressed via the Helmholtz free energy, F , and for monodisperse rigid particles the solutions to this are well known (see e.g. [21, 22]). Extending the theory to polydisperse systems requires the addition of an extra mixing term to the Helmholtz free energy [2, 7]. Flexibility may be incorporated in numerous ways (see e.g. [11–15]), and in this supplementary material, we build on the work of Wessels and Mulder [15] to produce a model describing binary systems of semi-flexible rods.

We consider a suspension of N_i semi-flexible rods of species $i = 1, 2$ with contour lengths L_i , in a volume V at temperature T . Following Wessels and Mulder [15] we model a rod of species i as a chain of M_i rod-like segments of length $l_i = L_i/M_i$ and diameter $D_i \ll l_i$. Denoting the orientation of the m -th segment by a unit-vector ω_m (with $1 \leq m \leq M_i$), we write the bending energy of a chain of species i with orientation $\mathbf{\Omega} = \{\omega_1, \dots, \omega_{M_i}\}$ as

$$U_i(\mathbf{\Omega}) = \sum_{m=1}^{M_i-1} u_i(\omega_m, \omega_{m+1}) = -\frac{P_i}{l_i} \sum_{m=1}^{M_i-1} \omega_m \cdot \omega_{m+1}, \quad (7)$$

where the stiffness is described in terms of the persistence length P_i [15]. Here and below we use thermal energy units by setting $k_B T = 1$. The state of the suspension is characterized by the orientation distributions functions (ODFs) $f_i(\mathbf{\Omega})$, which satisfy the normalization condition $\int d\mathbf{\Omega} f_i(\mathbf{\Omega}) = 1$ where $d\mathbf{\Omega} = \prod_{m=1}^{M_i} d\omega_m$. Denoting the total number of rods by $N = N_1 + N_2$, the density by $\rho = N/V$, and the mole fraction of species i by $x_i = N_i/N$, we can write the variational free-energy functional $F[f_1, f_2]$ of this system within an Onsager-like second virial approximation as

$$\begin{aligned} \frac{F}{N} &= \ln(B\rho) - 1 + x_1 \ln x_1 + x_2 \ln x_2 \\ &+ \sum_{i=1}^2 x_i \int f_i(\mathbf{\Omega}) \left(\ln(4\pi f_i(\mathbf{\Omega})) + U_i(\mathbf{\Omega}) \right) d\mathbf{\Omega} \\ &+ \frac{\rho}{2} \sum_{i,j=1}^2 x_i x_j \int f_i(\mathbf{\Omega}) f_j(\mathbf{\Omega}') K_{ij}(\mathbf{\Omega}, \mathbf{\Omega}') d\mathbf{\Omega} d\mathbf{\Omega}'. \end{aligned} \quad (8)$$

The first line of Eq. (8) represents the translational and the mixing ideal-gas contributions (with $B = \frac{\pi}{4} D_1 L_1^2$, a constant), the second line, the orientation entropy and bending energy, and the third line the excluded volume interactions given by

$$\begin{aligned} K_{ij}(\mathbf{\Omega}, \mathbf{\Omega}') &= \sum_{m=1}^{M_i} \sum_{m'=1}^{M_j} k_{ij}(\omega_m, \omega_{m'}) \\ &= l_i l_j (D_i + D_j) \sum_{m=1}^{M_i} \sum_{m'=1}^{M_j} |\sin \gamma(\omega_m, \omega_{m'})|, \end{aligned} \quad (9)$$

with $\gamma(\omega_m, \omega_{m'}) = \arccos(\omega_m \cdot \omega_{m'})$ the angle between chain segments [15] m and m' . The free-energy functional of Eq. (8) is a two-component generalization of the one-component segmented-chain functional of Ref.[15], and for $M_i = 1$ and $U_i \equiv 0$ it reduces to the Onsager functional for binary mixtures of rigid rods [7, 16].

At a given thermodynamic state point, the equilibrium ODFs minimize F and therefore satisfy the Euler-Lagrange equations $\delta(F - \mu_i N_i)/\delta f_i(\mathbf{\Omega}) = 0$ for $i = 1, 2$, with μ_i the chemical potential-like Lagrange multiplier that ensures a proper normalization. This gives rise to

$$f_i(\mathbf{\Omega}) = \frac{\exp(-U_i(\mathbf{\Omega}) - V_i(\mathbf{\Omega}))}{Q_i}, \quad (10)$$

$$V_i(\mathbf{\Omega}) = \rho \sum_{j=1}^2 x_j \int K_{ij}(\mathbf{\Omega}, \mathbf{\Omega}') f_j(\mathbf{\Omega}') d\mathbf{\Omega}', \quad (11)$$

where $V_i(\mathbf{\Omega})$ can be seen as a self-consistent field acting on all segments of a chain, and Q_i is a partition function-like normalization factor. Explicitly solving Eqs. (10) and (11) for state points of interest would be prohibitively expensive computationally because of the high-dimensional angular $\mathbf{\Omega}$ -grids that would be required in the case when $M_i \gg 1$. Instead, we formally evaluate the functional F of Eq. (8) in its minimum by inserting the solutions f_i of Eqs. (10) and (11) to find the equilibrium free energy

$$\frac{F_{\text{eq}}}{N} = \ln(B\rho) - 1 + x_1 \ln \frac{x_1}{Q_1} + x_2 \ln \frac{x_2}{Q_2} - \frac{1}{2} \rho \sum_{i,j} x_i x_j \sum_{m=1}^{M_i} \sum_{m'=1}^{M_j} \int k_{ij}(\omega, \omega') f_{i,m}(\omega) f_{j,m'}(\omega') d\omega d\omega', \quad (12)$$

where $f_{i,m}(\omega)$ is the ODF of the m -th segment ($m = 1, \dots, M_i$) of a chain of species $i = 1, 2$ defined by

$$f_{i,m}(\omega_m) = \int f_i(\mathbf{\Omega}) d\omega_1 \dots d\omega_{m-1} d\omega_{m+1} \dots d\omega_{M_i}. \quad (13)$$

Eq. (12) implies that the thermodynamics does *not* require the full solutions $f_i(\mathbf{\Omega})$ but in fact only the M_i single-segment distributions $f_{i,m}(\omega)$ and the normalization factors Q_i , for which an efficient iterative recursion scheme, that exploits the connectivity of the chain, can be set up as follows.

Eqs. (9) and (11) allow us to write $V_i(\mathbf{\Omega}) = \sum_{m=1}^{M_i} v_i(\omega_m)$ with the *same* selfconsistent field

$$v_i(\omega_m) = \rho \sum_{j=1}^2 \sum_{m'=1}^{M_j} x_j \int k_{ij}(\omega_m, \omega_{m'}) f_{j,m'}(\omega_{m'}) d\omega_{m'}, \quad (14)$$

for all segments of chains of the same species. As a consequence, Eq. (10) combined with Eq. (13) can be written as

$$f_{i,m}(\omega) = \frac{1}{Q_i} q_{i,m}(\omega) \exp[-v_i(\omega)] q_{i,M-m+1}(\omega), \quad (15)$$

with the partial-chain partition function

$$q_{i,m}(\omega_m) = \int \prod_{n=1}^{m-1} \exp[-v_i(\omega_n) - u_i(\omega_n, \omega_{n+1})] d\omega_n. \quad (16)$$

In the formulation of Eq. (15) the m -th segment ODF is seen as the statistical weight $\exp(-v_i(\omega))$ of that segment in the (selfconsistent) field $v_i(\omega)$, combined with the weights $q_{i,m}$ and $q_{i,M-m+1}$ of the two sub-chains from segment $m \pm 1$ to the two chain ends, respectively. Interestingly, the connectivity of the chain allows us to rewrite Eq. (16) as the recursion relation

$$q_{i,m}(\omega) = \int q_{i,m-1}(\omega') \exp[-v_i(\omega') - u_i(\omega', \omega)] d\omega' \quad (17)$$

such that a loop can be set up that (i) starts with a guess for $v_i(\omega)$ for $i = 1, 2$, (ii) solves for $q_{i,m}(\omega)$ for all $i = 1, 2$ and $m = 1, \dots, M_i$ using Eq. (17) together with $q_{i,1}(\omega) \equiv 1$, (iii) computes $f_{i,m}(\omega)$ and the normalization factor Q_i from Eq. (15), (iv) recalculates $v_i(\omega)$ using Eq. (14) and repeats (ii)-(iv) until convergence is found. Note that this scheme *only* requires an angular grid for ω , which in the light of the azimuthal and up-down symmetry of the isotropic and nematic phases of interest here, reduces to a single grid for the polar angle $\theta \in (0, \pi/2)$. The *only* difference

with Onsager-type theories for rigid-rod mixtures is the additional calculation and storage of $q_{i,m}(\omega)$ for $1 \leq m \leq M_i$ here. With the ODFs known, F_{eq} may be calculated from Eq. (12). The osmotic pressure is then calculated from $\Pi = \rho^2 \frac{\partial F_{\text{eq}}/N}{\partial \rho}$. For a binary system, phase behavior is most easily analyzed using the Gibbs energy per particle, $\tilde{g}(x, \Pi) = \frac{F_{\text{eq}}}{N} + \frac{\Pi}{\rho}$. By fixing Π , \tilde{g} may be calculated as a function of x_2 (with $x_1 = 1 - x_2$), and performing a common tangent construction allows for the prediction of coexisting phases [2, 7, 23]. For the special case of a monodisperse system, we simply set $x_2 = 0$.

We may also calculate the nematic order parameters, $S_{i,m}$, which define the local order of the m -th segment

$$S_{i,m} = \int d\omega f_{i,m}(\omega) P_2(\omega \cdot \mathbf{n}), \quad (18)$$

where $P_2(\omega \cdot \mathbf{n})$ is the second Legendre polynomial, and \mathbf{n} is the nematic director. We define the nematic order of a rod as the average nematic order along the chain

$$S_i = \frac{1}{M_i} \sum_{m=1}^{M_i} S_{i,m}. \quad (19)$$

Effective length

The calculation of the effective length goes as follows. We define the mean square effective length $L_{e,i}^2$ as

$$\begin{aligned} L_{e,i}^2 &= l_i^2 \sum_{m=1}^{M_i} \sum_{m'=1}^{M_i} \langle \omega_m \cdot \omega_{m'} \rangle \\ &= l_i^2 \sum_{m=1}^{M_i} \sum_{m'=1}^{M_i} \int (\omega \cdot \omega') f_{i,m,m'}(\omega, \omega') d\omega d\omega', \end{aligned} \quad (20)$$

where we are summing the squares of the average length projections of all chain segments m' along the director of all segments m . Here, $f_{i,m,m'}(\omega, \omega')$ is the pair orientational distribution function (PDF) defined by

$$f_{i,m,m'}(\omega, \omega') = \int f_i(\boldsymbol{\Omega}) \delta(\omega_m - \omega) \delta(\omega_{m'} - \omega') d\boldsymbol{\Omega}, \quad (21)$$

where we are integrating out all other degrees of freedom from $f_i(\boldsymbol{\Omega})$ except those of segments m and m' . Note that $f_{i,m,m'}(\omega, \omega')$ is the probability that a chain of species i is in a configuration with the m -th and m' -th segment having orientations ω and ω' , simultaneously. Inserting Eq. (10) into Eq. (21), and using Eqs. (14) and (16), we find that

$$f_{i,m,m'}(\omega, \omega') = \frac{1}{Q_i} q_{i,m}(\omega) \exp[-v_i(\omega)] Q_{i,m,m'}(\omega, \omega') \exp[-v_i(\omega')] q_{i,M-m'+1}(\omega'), \quad (22)$$

with the same notation as before. Here $Q_{i,m,m'}(\omega, \omega')$ is the partial chain partition function that takes into account the effect of the chain segments that link segment m and segment m' . For neighboring segments $m' = m + 1$ we have $Q_{i,m,m'}(\omega, \omega') = \exp[-u_i(\omega, \omega')]$, and for $m' = m + 2 \dots M$, it follows the recursion relation

$$Q_{i,m,m'}(\omega, \omega') = \int d\omega'' Q_{i,m,m'-1}(\omega, \omega'') \exp[-v_i(\omega'')] \exp[-u_i(\omega'', \omega')]. \quad (23)$$

By construction, each pair orientation distribution function also obeys the normalization condition $\int f_{i,m,m'}(\omega, \omega') d\omega d\omega' = 1$. As we already know the ODFs, and hence $q_{i,m}(\omega)$ and $v_i(\omega)$, from our phase diagram calculations, the calculation of the PDFs and $L_{e,i}$ is relatively straight forward. We use $L_{e,i}$ to calculate the diameter $D_{e,i}$ required for rigid rods to have the same excluded volume as our flexible rods, at the same state point, obtaining the effective shape of the rods.

fd virus parameters and values

In order to accurately describe semi-flexible rods, we must ensure that we are in the continuum limit. That is, we must use a sufficient number of chain segments to ensure that our results capture the physics of a continuous chain. We do this by checking the convergence of our results with increasing M_i at fixed P_i , by adapting $l_i = L_i/M_i$. We shall now examine the one-component system fd virus system, and hence we drop the subscript i . In Fig. 4, we show the isotropic (I) and nematic (N) equation of state of a one-component fd virus system, for various M values, starting from the rigid-rod limit $M = 1$. Clearly, the isotropic branch is independent of M , while the nematic branch strongly depends on M . The I-N coexistence, which is represented by the jump, shows a phase transition that shifts to higher ρ and Π upon increasing M , reaching a well-defined continuum limit in the pressure regime of interest for $M \geq 15$. Coexistence is found at $\Pi B = 29.54$.

Varying the stiffness of semi-flexible rods can have a large effect on the properties of the nematic phase at coexistence. Fig. 5 shows the equation of state for bio-engineered fd virus particles of various persistence lengths. We see that coexistence is found at much lower densities (and osmotic pressures) for stiff rods than for flexible ones, in agreement with Refs. [11–15].

We may also calculate the nematic order parameter of each chain segment in a rod from Eq. (18). Fig. 6 shows the nematic order parameter S at a distance $r \in [0, L]$ along the rod, at isotropic-nematic coexistence for fd virus particles of various persistence lengths. We see that rigid rods are more ordered at coexistence than flexible rods, despite coexistence being found at a lower density. The chain segments in the middle of the rods are also found to be more ordered than the end segments, in agreement with earlier bifurcation findings in Ref. [15].

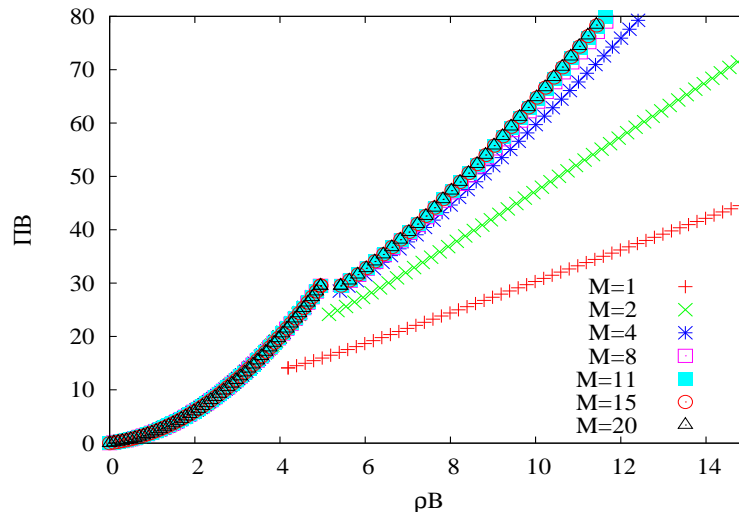


FIG. 4. Convergence of equation of state in $\rho B - \Pi B$ representation, for increasing number of chain segments M for fd virus parameters $L = 0.88\mu\text{m}$, $D = 6.6\text{nm}$ and $P = 2.2\mu\text{m}$. We find that $M = 15$ is within the continuum limit for the fd virus.

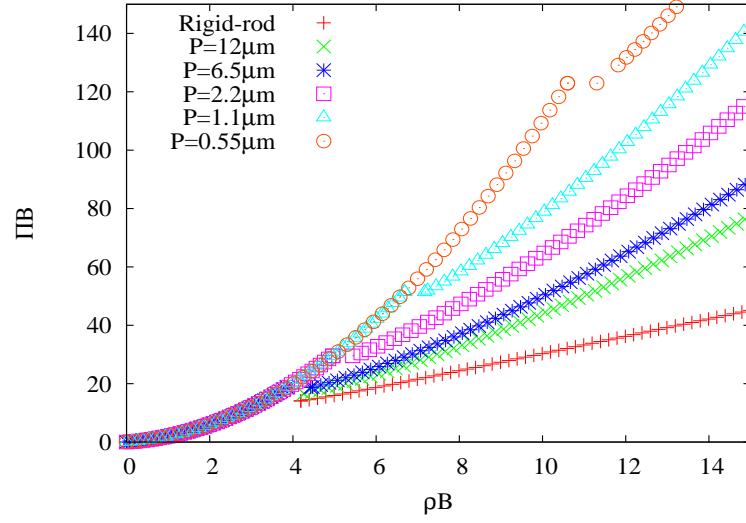


FIG. 5. Equation of state in $\rho B - \Pi B$ representation, for fd virus dimensions $L = 0.88\mu\text{m}$, $D = 6.6\text{nm}$ and varying persistence length P .

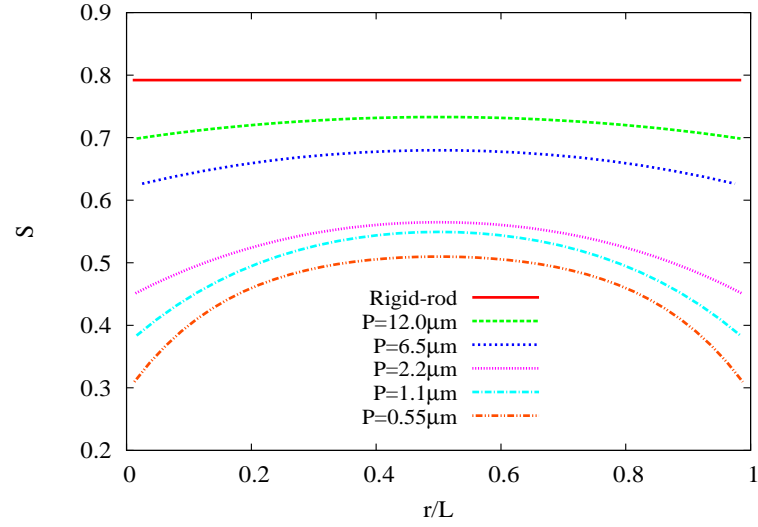


FIG. 6. Nematic order parameter S of fd virus particles of various persistence lengths, at a distance $r \in [0, L]$ along the rod. The densities of the nematic phase at coexistence are: $\rho B = 4.19$, $\rho B = 4.27$, $\rho B = 4.42$, $\rho B = 5.45$, $\rho B = 7.17$ and $\rho B = 11.30$ for $P \rightarrow \infty$ (rigid-rod), $P = 12\mu\text{m}$, $P = 6.5\mu\text{m}$, $P = 2.2\mu\text{m}$, $P = 1.1\mu\text{m}$ and $P = 0.55\mu\text{m}$, respectively.